King Saud University

Arabian Journal of Chemistry

www.ksu.edu.sa
www.sciencedirect.com

ORIGINAL ARTICLE

Identification of pyrrolizidine alkaloids and flavonoid glycosides through HR-LCMS/MS analysis, biological screening, DFT and molecular docking studies on *Heliotropium dasycarpum* Ledeb.

Mahreen Mukhtar [a], Muhammad Saleem [a], Mamona Nazir [b], Naheed Riaz [a], Nusrat Shafiq [c], Hammad Saleem [d], Saba Tauseef [e], Saima Khan [a], Muhammad Ehsan Mazhar [f], Rasool Bakhsh Tareen [g], Mian Habib ur Rahman Mahmood [h], Muhammad Imran Tousif [h,*], Suvash Chandra Ojha [i,j,*]

[a] *Institute of Chemistry, Baghdad-ul-Jadeed Campus, The Islamia University of Bahawalpur, 63100 Bahawalpur, Pakistan*
[b] *Department of Chemistry, Government Sadiq College Women University, Bahawalpur, 63100 Bahawalpur, Pakistan*
[c] *Department of Chemistry, Government College Women University, Faisalabad 38000, Pakistan*
[d] *Institute of Pharmaceutical Sciences (IPS), University of Veterinary & Animal Sciences (UVAS), Lahore 54000, Pakistan*
[e] *Dr. Panjwani Center for Molecular Medicine and Drug Research, International Center for Chemical and Biological Sciences, University of Karachi, Karachi, Pakistan*
[f] *Department of Physics, Bahauddin Zakariya University Multan, Pakistan*
[g] *Department of Botany, Baluchsitan University Quetta, Pakistan*
[h] *Department of Chemistry, Division of Science and Technology, University of Education Lahore, Pakistan*
[i] *Department of Infectious Diseases, The Affiliated Hospital of Southwest Medical University, Luzhou 646000, China*
[j] *Southwest Medical University, Jiangyang District, Luzhou 646000, Sichuan, China*

* Corresponding authors at: Department of Infectious Diseases, The Affiliated Hospital of Southwest Medical University, Luzhou 646000, China (S.C. Ojha).
E-mail addresses: imran.tousif@ue.edu.pk (M.I. Tousif), suvash_ojha@swmu.edu.cn (S.C. Ojha).
Peer review under responsibility of King Saud University.

Production and hosting by Elsevier

Abstract The current study was carried out to reveal the chemical profile and biological screening of *Heliotropium dasycarpum* Ledeb, as well as the feasibility of its industrial application. Therefore, the methanolic extract (HdM) of *H. dasycarpum* was divided into n-hexane (HdH), ethyl acetate (HdE) and water (HdW) soluble fractions. All the fractions were inactive against acetylcholinesterase (AChE) enzyme, 3T3 and HeLa cell lines, but showed immunomodulatory effect up to 37 %. HdE fraction further displayed significant anti-urease activity with IC_{50} value of 74. 072 ± 0.002, while HdM was found moderate inhibitor (63 %). Thus HdE was subjected to HR-LCMS/MS analysis in positive and negative ionization modes, and a qualitative analytical method with a data mining strategy was utilized. The secondary metabolites were identified by dereplication strategy using molecular networking as a bioinformatics tool, which disclosed the presence of 08 known alkaloids of heliotrine-type (**1, 3, 5–10**), and 05 (**12–16**) known flavonoids and flavonoid glycosides along with 03 new (**2, 4** and **11**) putative pyrrolizidine analogues. DFT simulations of identified compounds were performed using multiple quantum chemical and geometrical descriptors in order to determine their quantitative structure activity relationship. These secondary metabolites were docked against the enzyme urease which substantiated the inhibitory action of pyrrolizidine alkaloids and flavonoid glycosides. Furthermore, ADME analysis provided the base for the use of these compounds for further studies as drug leads and to unveil industrial application of *H. dasycarpum* in formulating products against gastritis, peptic ulcer and gastric cancer.

1. Introduction

Heliotropium dasycarpum of Boraginaceae is a perennial plant found in Southern Punjab, Blaochistan, Gilgit and Waziristan in Pakistan. Locally known as Sagdaroo; it shows various biological effects like cytotoxicity, pesticidal, anti-fungal and enzyme inhibitory activities (Ghaffari et al., 2013; Ghaffari et al., 2016). Use of fresh extract of *H. dasycarpum* to cure eye diseases in animals is common practice in local community (Tareen et al., 2010). Previous phytochemical studies on *Heliotropium* species disclosed the occurrence of pyrrolizidine alkaloids (PAs), which are commonly found in variety of toxic plants around the globe and are possibly a source of poisoning in livestock, wildlife, and also in humans, through herbal folk medicines (Chen et al., 2019). They are toxic to liver and sometimes considered as carcinogenic (Chen et al., 2010). They are potent hepatotoxic, antimitotic (Seremet et al., 2018; Schramm et al., 2019), teratogenic, mutagenic and carcinogenic agents (Fayed, 2021). Typically PAs exist as esters in the plants of the Boraginaceae family (Shimshoni et al., 2015). Almost 700 pyrrolizidine alkaloids have been isolated from various plants (Woodley, 2018).

Although, *H. dasycarpum* is ecologically very important plant, which is being used in folk medicine system, very little information about its metabolite's biological effects is available. In the present study, the MeOH extract (HdM) of *H. dasycarpum* was divided into hexane (HdH), ethyl acetate (HdE) and water (HdW) soluble fractions, which were evaluated for various bioactivities, besides, the study discloses the presence of pyrrolizidine alkaloids and flavonoid glycosides through dereplication technique based on the MS/MS and molecular networking. HdM, HdH, HdE and HdW fractions were tested for their bioactive potential. The HdE exhibited significant inhibitory activity against the enzyme urease. Therefore, selected compounds identified in the extract were docked against urease for mapping its inhibitory action along with the ADME studies.

Urease enzyme aids in colonizing of *Helicobacter pylori* in stomach by hydrolyzing urea into ammonia, which reacts with chloride ions giving toxic compounds. Thus *H. pylori* is responsible for stomach infections by accelerating the oxidation in human neutrophils and accumulate free radicals (hydrogen peroxide which oxidize chloride ions). Therefore, urease inhibition is required to prevent the colonization of *H. pylori* in the stomach. Side effects and induced resistance of antibiotics urges to explore the urease inhibitors from the safe natural resources, like plants (Ghaffari et al., 2016; Fox Ramos et al., 2017).

The isolation of bioactive constituents from plants is costly and time consuming process, even if it is bioactivity guided isolation, the known compounds are always re-isolated. Dereplication strategy of medicinal plant is now in trend as it saves from the wastage of resources and time. Dereplication of mass spectrometric data by Molecular Networking (MN) is an efficient approach to predict the new analogues of known natural products in a crude extract prior to isolation. MN clumps up all the similar molecular ions from MS experiment into a cluster, which helps to annotate the structures of known compounds by matching their mass spectra with online spectral libraries and forecasting the new analogues. Such MS-based paradigm in combination with the bioactivity of interest can revitalize the plants-based secondary metabolites program to target only the novel analogue(s) prior to the isolation and hence accelerating the process of discovery of new natural chemical components (Nothias et al., 2018). MN visualizes all the molecular ions generated and detected in an LC-MS/MS, formed into grouped nodes based on their MS^2 similarity connected by the edges in the form of a cluster. MN rely on the fact that structurally-related entities with the same basic structural skeleton tend to fragment in similar way; hence appear in the same constellation of ions, while heterogeneous chemicals get classified into a different sub network, providing base for rapid identification of their molecular families. The success of structural annotation depends on the databases and connected spectral libraries. *In-silico* predictor analyze thousands of samples in even less time, paving a targeted way to detect new secondary metabolites (Aman et al., 2020).

Thus, it was envisioned that *H. dasycarpum* reinvestigation by HR-LCMS/MS with aid of mass spectral networking could be a promising deal in pointing out possibly new compounds. Since the plant extract showed significant inhibition of urease enzyme, additional, molecular docking studies provided clear insight of compounds, interaction and binding with target protein (urease enzyme) in the form of binding energies. Molecular docking of compounds against protein predicts the mechanism of action and interaction between ligand and substrate.

The binding energies show interface of protein binding sites and the compound of interest (maximum the linkage, smaller the energy value) as the compound achieve the conformations with suitable orientation inside the active site of enzyme. Similar docking studies against urease enzyme are also reported by Moghimi et al., 2018 and Aman et al., 2020 (Moghimi et al., 2018; Aman et al., 2020).

2. Materials and methods

2.1. General experimental procedures

HR-LCMS/MS, and MS/MS experiments were performed on a Bruker TOF-MS MaXis Impact ESI-HR-MS. HPLC profiling was carried out using Waters system consisting of Waters Binary Pump 1525, integrated with a Waters plus auto-sampler 717, and a Waters photodiode Array Detector 2996, controlled by Empower 3 software. A Luna Omega Polar C18 column (3 μm, 250 × 4.6 mm) was employed to profile all the extracts using a flow rate of 0.7 mL/min.

2.2. Chemicals and materials

Acetonitrile HPLC grade was supplied by J. T. Baker (Germany) and Acetonitrile of MS grade was provided by Roth (Germany). Other chemicals were purchased from Fisher Chemical and Sigma Aldrich.

2.3. Collection of the plant material and extract preparation

H. dasycarpum Ledeb. was collected in July 2018 from Baluchistan University Campus Quetta, and was identified by Prof. Dr. Rasool Bakhsh Tareen, Department of Botany, University of Baluchistan, Quetta, Pakistan, where a voucher specimen number HD-RBT-05 has been deposited in the herbarium. The shade-dried plant material (3 kg) was extracted with distilled MeOH twice (5 L, room temp) and solvent was evaporated under reduced pressure to get 75 g of dark gummy mass. The methanolic extract (HdM 75 g) was suspended in distilled water (500 mL) and was extracted successively with hexane and ethyl acetate, to get hexane fraction (HdH, 35 g), ethyl acetate fraction (HdE, 22 g), while residual water fraction (HdW) was obtained as 16 g. Since HdE fraction exhibited significant anti-urease activity (section 3.1;

Table 1), it was analyzed by HR-LC-MS/MS to unveil its secondary metabolic picture.

2.4. Protocols for biological assays

All the fractions (HdM, HdH, HdE and HdW) were analyzed for their anti-cancer (3T3 cell line and NIH HeLa cell line), immunomodulatory, anti-urease, and anti-cholinesterases activities.

2.4.1. Immunomodulatory bioassay

Luminol-enhanced chemiluminescence assay was done, as previously reported method (Helfand et al., 1982). Test was performed in half area 96 well plates, in which 25 μL of diluted whole blood HBSS + + (Hanks Balanced Salt Solution, containing calcium chloride and magnesium chloride) (Sigma, St. Louis, MO, USA) was added and incubated with 25 μL of three different concentrations of test sample (1, 10 and 100 μg/mL), each in triplicate. Control wells contained only HBSS + + and cells. Plate was incubated at 37 °C for 15 min in the thermostat chamber of luminometer. Drug ibuprofen was used as positive control. After incubation, 25 μL of serum opsonized zymosan (SOZ) (Fluka, Buchs, Switzerland) and 25 μL of intracellular reactive oxygen species detecting probe, luminol (Research Organics, Cleveland, OH, USA), were added into each well, except blank wells (containing only HBSS + +). The level of ROS was recorded by a luminometer and expressed as relative light units (RLU) (Rahman et al., 2016).

2.4.2. Cytotoxic (3T3 cell line and HeLa cell line) assays

Test was performed in 96-well flat-bottomed micro plates using standard MTT (3-[4, 5-dimethylthiazole-2-yl]-2,5-diphenyl-tetrazolium bromide) colorimetric assay (Ahmad et al., 2016). Under necessary conditions, 3T3 cells and HeLa cell lines (fibroblast NIH and cervical cancer cells) were cultured, harvested and counted with haemocytometer. It was diluted with required medium. Cell culture was prepared having concentration of 5×10^4 cells/ml and shifted to (100 μL/cell) 96-well plates. After overnight incubation, medium was wasted and 200 μL of fresh medium was added with defined concentrations of plant samples. After 48 h, 200 μL MTT (0.5 mg/ml) was added to each well and incubated additionally for

Table 1 Biological Activities of the extracts of *H. dasycarpum*.

Test Samples	Immunomodulatory	Hela cell line	3T3 cell line	Urease	AChE
	% Inhibition*	% Inhibition*	% Inhibition*	IC_{50} μg/mL	% Inhibition
HdM	32.18 ± 0.18	2	2	–	37.62 ± 0.15
HdH	22.92 ± 0.16	1	1	–	19.42 ± 0.13
HdE	37.10	2	2	74.072 ± 0.02	5.8 ± 0.12
HdW	19.66 ± 0.19	1	1	–	16.45 ± 0.12
Iboprofen**	73.2	1.2 ± 0.8	–	–	–
Doxorubicin**	–	71	–	–	–
Cyclohexamide**	–	–	71	–	–
Thiourea**	–	–	–	21.31 ± 0.14	–
Eserine**	–	–	–	–	91.27 ± 1.17

*Concentration of all the extracts were 30 μg/mL.
**Reference/Standard drug used in respective assay.
All experiments were performed in triplicates and final values calculated as means of the three readings in each case.

4 h. Afterwards, 100 µL of DMSO was added to each well Micro plate reader (Spectra Max plus, Molecular Devices, CA, USA) used to measure reduction of MTT by calculating absorbance at 540 nm. 50% growth inhibition (IC_{50}) and % inhibition was recorded using Soft- Max Pro software (Molecular Device, USA).

2.4.3. Enzyme inhibition assays

For enzyme inhibition potential of the extract, different *in vitro* assays were performed against urease and cholinesterase (AChE) enzymes using previously reported methods (Tahseen et al., 2010; Lazarova et al., 2015). Antiurease assay was performed through Berthelot method: the phosphate buffer (6 mL) solution was added into 20 mL of urease enzyme in wells of 96-well-plate. After incubation at 25 °C for 10 min the test sample was added in it. Further incubation at room temperature, 15 mL of 20 mM urea was added, and was further incubated at 25 °C for 10 min; followed by the addition of 100 mL RGT 2 (rainbow trout gonad cell line-2). Whole reaction mixture was again incubated at room temperature for 25 min and absorbance was measured on ELISA reader by using Gen 5 software at 630 nm. The percentage inhibition was calculated by using the following formulae and IC_{50} values of samples were calculated using EZ-Fit Enzyme Kinetics Software (Perrella Scientific Inc., Amherst, MA, USA).

$$\text{Inhibition}(\%) = \text{Control} - \text{Test} \times 100/\text{Control}$$

2.5. LC-MS/MS data acquisition

HR-LCMS/MS data was acquired in both positive and negative ionization modes. HPLC-method was applied as follows: with 0.1% formic acid in H_2O as solvent A and acetonitrile as solvent B, with gradient of 10 to 100% B for 45 min, using a flow rate of 0.5 mL/min; 3 µL injection volume and UV detector at 190–800 nm. A capillary voltage of 4500 V, nebulizer gas pressure (nitrogen) of 2 bar, ion source temperature of 200 °C, dry gas flow of 8 L/min source temperature, and spectral rates of 1 Hz for MS^1 and 1 Hz for MS^2 were used. For acquiring MS/MS fragmentation, the 10 most intense ions per MS^1 were selected for subsequent CID with stepped CID energy applied. Sodium formate was used as an internal calibrant. Data processing was performed using Bruker Daltonics Data Analysis 4.2.

2.5.1. Data processing and generating molecular networking

All the MS/MS data were imported into MetaboScape 3.0 and the mgf files were uploaded in different jobs to the GNPS web server (https://gnps.ucsd.edu). The molecular network was generated as follows: parent mass tolerance 0.05 Da, ion tolerance 0.05 Da, min pairs Cos 0.7, min matched fragment ions 6, minimum cluster size 2, and maximum connected component size 100. Advanced library search options were set to a library search min matched peaks 6, score threshold 0.7, search analogs set to Don't Search. All other settings were left default.

2.5.2. Visualizing and annotation of the molecular networks

Molecular network was visualized using Cytoscape 6.02, comprised of nodes of neutral masses. Color mapping allowed marking the fractions in different colors showing the percentage of that specific ion in a specific fraction and size of the nodes was adjusted according to the intensity of ion. Many clusters were chosen randomly to be annotated from each MN. First, the retention time and the mass of each node were checked in the raw data to validate the ion identity. After that, the MS/MS spectra were imported into Sirius + CSI:FingerID that was implemented with databases named as Derep, Marinlit and Pubchem to predict the possible molecular formula using the suggested fragmentation trees. Finally, the putative molecular formula hit was checked in the literature to see if this compound is coming from plant sources, and the name of the origin sample was compared with the name in the literature.

2.6. Data processing for molecular docking

The study of binding interactions of known compound and new analogs were done by using AutoDock 4.2 package (Morris et al., 2009). The Lamarckian genetic algorithm was applied for 25×10^6 energy evaluations for 10 runs. The PDB structure 3LA4 downloaded from RCSB PDB (Sussman et al., 1998) for Jack bean urease enzyme was used as target protein. Chem3D Ultra was used to sketch the three new analogs and known compounds i.e. 5′ deoxylasiocarpine, and Neochilenin and saved in pdb format. All other compounds were downloaded as sdf files from PubChem (Lasiocarpine PubChem CID 5281735, Thiourea PubChem CID 2723790, Punctanecine PubChem CID 134715006, Heliotrine PubChem CID 906426, Acetyleuropine PubChem CID. 101915798 Quercetin-3-O-glucoside PubChem CID 5280804). All the compounds along with new analogs were then energy minimized using Frog2 online server (Miteva et al., 2010). The grid box consisted of $108 \times 80 \times 86$ with grid spacing 0.375A° and covered nickel and active residues of enzyme. The docked conformations were evaluated on root mean square deviation value (RMSD) also known as docking score or binding energy. The conformation having lowest docking score was further evaluated for 2D interaction via PoseView, and for 3D interactions through chimera and ezCADD (Tao et al., 2018).

2.7. ADME/Tox analysis of the compounds

The ADME/Tox analysis (Absorption, Distribution Metabolism, Excretion and Toxicity) using FAF *Drugs*4 at Mobyle@rpbs server was performed for thiourea, the known inhibitor and all the compound. The 3D sdf format of inhibitor and compounds retrieved from PubChem while new analogs were converted into format through Open Babel. The inhibitor and compounds were submitted at the server.

2.8. DFT studies in scope of quantitative structure activity relationship (QSAR)

Density functional theory (DFT) calculations have been performed utilizing software Gaussian09 supported by the Gauss view 6.0. For all the calculations, the B3LYP functional and the 6-311G(d,p) basis set have been utilized (Rahman et al., 2020). In result of DFT calculations, HOMO-LUMO geometries, energy gap, dipole moment, net charge and other computational parameters were obtained (Ozdemir et al., 2015). Geometrical and quantum based computational descriptors

obtained via DFT calculations having B3LYP/6311-G basis set to assist SAR studies of under studied molecules is revealed in Table 6.

3. Results and discussion

Literature survey revealed that *Heliotropium* plants produce various classes of secondary metabolites belonging to pyrrolizidine group of alkaloids (Shimshoni et al., 2015), flavonoids (Singh et al., 2017), phthalates (Demıray et al., 2013), and steroids (Sarkar et al., 2021), most of which are bioactive compounds, especially the pyrrolizidine alkaloids and flavonoids. Chemical tests showed that the methanolic extract (HdM) of *H. dasycarpum* is rich in alkaloids and phenolics; therefore, it was divided into solvent-polarity based different fractions, which were screened for anticancer, immunomodulatory and enzyme inhibition activities.

3.1. Biological screening of the extracts

Literature reports further disclosed that the pyrrolizidine alkaloids or the plant extracts rich in these alkaloids showed cytotoxic activities against different cell lines (Singh et al., 2002; Nibret et al., 2009; Gao et al., 2020), however, in the present study, the fractions HdM, HdH, HdE, and HdW of *H. dasycarpum* were inactive against 3T3 and HeLa cell lines up to concentration of 30 μg/mL (Table 1). Generally our results were contrary to the literature reports, however, one published report revealed that Achakzai et al also evaluated cytotoxic activities of different extracts of *Heliotropium europaeum* against MCF-7, 3T3 and HeLa cell lines and found inactive; also in brine shrimp lethality assay, all the extracts were observed inactive (Achakzai et al., 2020). This report supports our study and substantiates a non-toxic nature of *H. dasycarpum*, however, it may show anticancer activities against
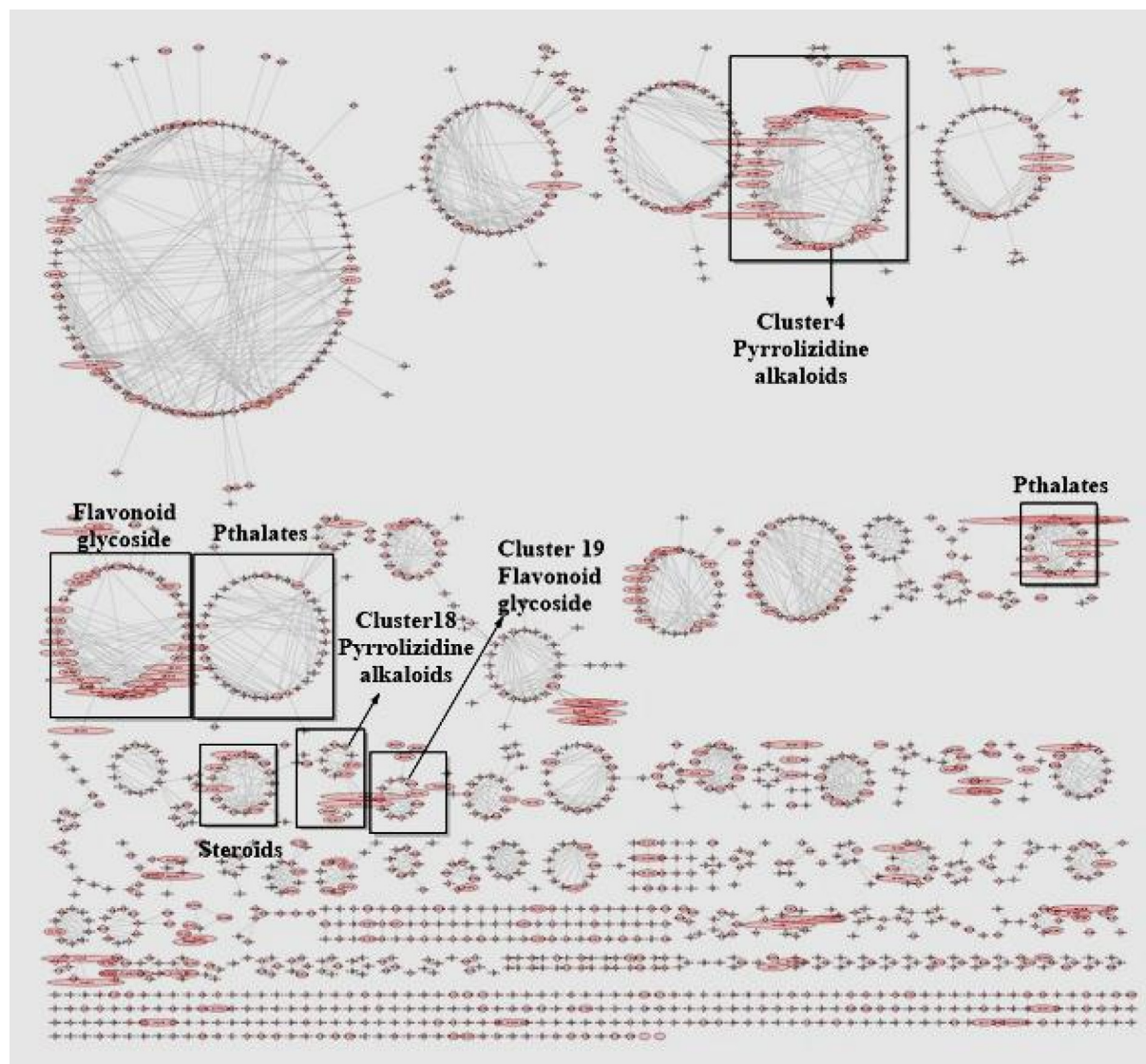
Fig. 1 Molecular network depicting the intensity of the molecular ion in clusters, clusters are identified as same type of fragments tend to occur together giving a tentative idea about class of compounds.

other cell lines. HdM, HdH, HdE, and HdW were also tested against acetylcholinesterase enzyme (AChE), where only HdM exhibited 37.62 % inhibition, while other fractions were inactive. In immunomodulatory assay, all the fractions showed weak effects (Table 1). Against urease enzyme, only HdE was noticed as significant inhibitor with IC_{50} value of 74.072 ± 0. 02 μg/mL (Table 1), which is comparable with the inhibitory activity of thiourea with IC_{50} value of 21.31 ± 0.14 μg/mL (standard inhibitor). In the same assay, HdM was found as weak inhibitor, whereas, other extracts were inactive. Ghaffari et al studied anti-urease activity of methanolic and DCM extracts of *H. dasycarpum*, which has been reported to be very weak (Ghaffari et al., 2016), but in our studies, methanolic extract (HdM) moderately inhibited urease activity, while ethyl acetate fraction (HdE) was found significant inhibitor. The weak inhibitory potential of HdM could be compensated due to suppression of amount of active components pyrrolizidine alkaloids and flavonoids, which is higher in HdE. Since in referred work (Ghaffari et al., 2016), DCM extract was studied, where pyrrolizidine alkaloids and flavonoid glycosides might not have been extracted with DCM, and thus reported as inactive, therefore, the anti-urease activity, in our studies, could be attributed to the presence of higher concentration of pyrrolizidine alkaloids and partly to the flavonoid glycosides in ethyl acetate fraction HdE (Table 1).

3.2. Interpretation of molecular network

Keeping in view the significant antiurease activity of HdE, it was subjected to LC-HRMS/MS (in positive and negative ion modes) analysis to unveil chemical picture of this fraction. In negative mode, a poor fragmentation was obtained therefore, based on the fragmentation patterns of standards investigated in positive tandem mass spectrometry (MS/MS), molecular net-

work was generated, where MS/MS spectra were arranged into 230 nodes compromising 51 clusters of connected nodes (Fig. 1). The initial screening of the generated molecular network (Fig. 1) allowed quick dereplication of the previously reported 8 alkaloids of heliotrine-type (1, 3, 5–10) with three new putative analogues (2, 4 and 11) (Scheme 1) and five (12–16) flavonoid derivatives (Scheme 2) in HdE of *H. dasycarpum*. Heliotrine-type PAs includes europine, heliotrine and lasio-carpine, which are the major components of the *Heliotropium* spp (Shimshoni et al., 2015; Chiesa et al., 2018). An overview of these compounds with their precursor ion, fragmentation ions and retention time is given in Table 2. Clusters were chosen and annotated on the basis of the ion intensity and the basic skeleton of class of compounds. The MS/MS fragmentation data showed the cleavage of the molecule of pyrrolizidine alkaloid giving characteristic fragment of necine base unit either at m/z 156 [M + H⁻] (Shimshoni et al., 2015), or in addition, ions at m/z 138 and 120 [M + H⁻] (Fig. 2), which suggested the ester type of pyrrolizidine alkaloids.

3.3. Structural annotation of clusters in molecular networking

Cluster 4 (Fig. 3) showed a node with m/z 411.2257, corresponding to the molecular formula $C_{21}H_{33}NO_7$. Diagnostic fragment ion at m/z 336.1816 $[C_{18}H_{26}NO_5]^+$ by the loss of $[C_3H_7O_2]^+$ was observed along with further fragment ions at m/z 220.1339 $[C_{13}H_{18}NO_2]^+$ due to the cleavage of weakly allylic ester bond and at m/z 120.0809 $[C_8H_{10}N]^+$. The loss of 102 Da, produce the fragment ion at m/z 120.0809 $[C_8H_{10}N]^+$ obtained through the loss of ester linkage [M⁺-$C_5H_9O_2$]. Giving an example pyrrolizidine alkaloids exhibit characteristic ions of m/z 220 and m/z 120 of due to the necine nucleus after the loss of the acid in C9 and C7. For lasio-carpine (1) the molecular ion peak is m/z 412.23376 [M + H]⁺, and the most abundant fragment ions were found to be
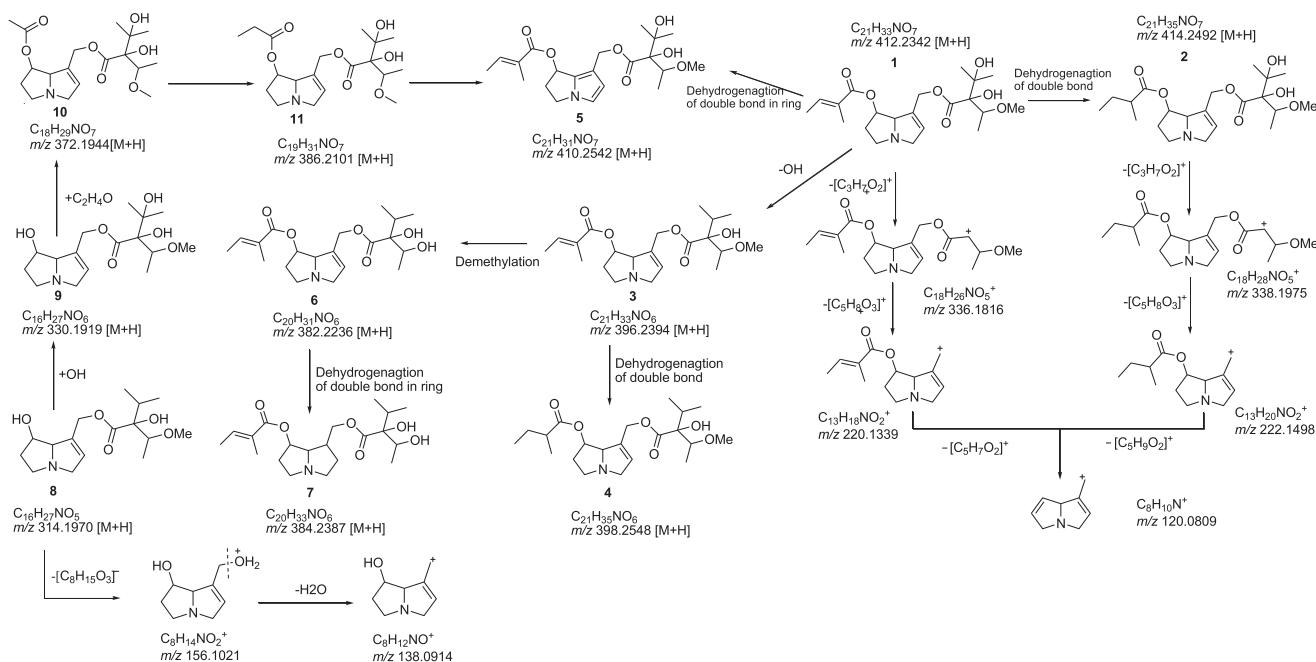
Scheme 1 Fragmentation pattern and Biosynthetic linkage of Pyrrolizidine alkaloids of Cluster 4 and 18.
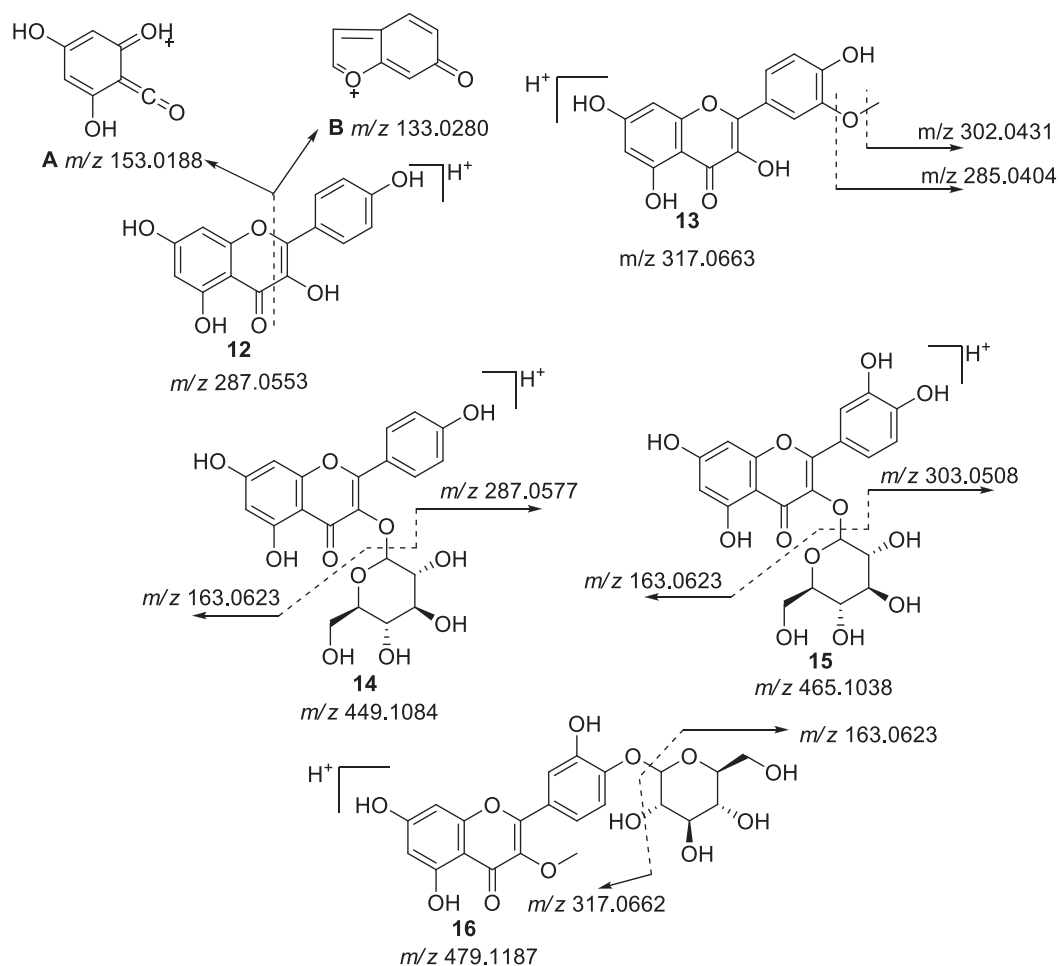
Scheme 2 Fragmentation pattern of flavonoid and flavonoid glycosides of Cluster 19.

Table 2 Structural annotation of compounds identified in Molecular Network Generated Form Fractions of *Heliotropium dasycarpum*.

Comp. No	RT	Molecular mass	Observed molecular ion in MS [M + H]	Fragments observed in MS/MS	Mol. Formula (error)	Proposed structure/identified compound
Cluster 4						
1	11.5	411.2257	412.2342	336.1816, 220.1339, 120.0809	$C_{21}H_{33}NO_7$ (-1.2)	Lasiocarpine
2	12.2	413.2413	414.2492	338.1975, 222.1498, 120.0811	$C_{21}H_{35}NO_7$ (-1.7)	New analogue of lasiocarpine
3	15.1	395.2338	396.2394	220.1341, 120.0810	$C_{21}H_{33}NO_6$ (-1.2)	5′-deoxylasiocarpine
4	15.7	397.2067	398.2548	222.1495, 120.0809	$C_{21}H_{35}NO_6$ (-0.7)	New analogue of 5′-deoxylasiocarpine
5	17.2	409.2482	410.2542	220.1339, 120.0809	$C_{21}H_{31}NO_7$	Dehydrolasiocarpine
6	12.6	381.2155	382.2236	220.1710, 120.0808	$C_{20}H_{31}NO_6$ (-3.0)	Symviridine or Symphytine,
7	13.7	383.2992	384.2387	220.1367, 120.0810	$C_{20}H_{33}NO_6$	Punctanecine
Cluster 18						
8	7.1	313.1895	314.1970	156.1021, 138.0914	$C_{16}H_{27}NO_5$ (-1.6)	Heliotrine
9	4.6	329.1841	330.1919	254.1394, 156.1024, 138.0916	$C_{16}H_{27}NO_6$ (-2.7)	Europine
10	7.4	371.1950	372.2233	312.1816, 154.0865, 136.0760	$C_{18}H_{29}NO_7$ (-2.0)	7-acetyleuropine
11	9.0	385.2101	386.2179	312.1812, 136.0759	$C_{19}H_{31}NO_7$ (-1.8)	New Analogue of 7-acetyleuropine
Cluster 19						
12	11.5	286.0553	287.0553	153.0188	$C_{15}H_{10}O_6$ (0.7)	Kaempferol
13	1.18	316.0583	317.0663	302.0431, 285.0404	$C_{16}H_{12}O_7$ (0.6)	Methoxy kaempferol
14	11.6	448.1006	449.1084	287.0577, 163.0623	$C_{21}H_{20}O_{11}$ (-1.6)	Kaempferol-3-O-glucoside
15	10.4	464.0955	465.1038	303.0508, 163.0623	$C_{21}H_{20}O_{12}$ (-2.2)	Quercetin-3-O-glucoside
16	11.8	478.1111	479.1187	317.0662, 285.1241	$C_{22}H_{22}O_{12}$ (0.4)	Neochilenin
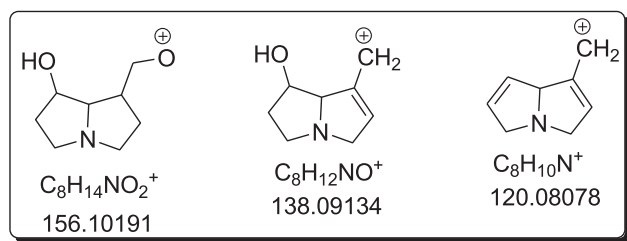
Fig. 2 Characteristic fragmentation of necine base unit.

m/z 120.08099 (100%) and m/z 220.13313 (20%), through mechanism of fragmentation involving a McLafferty-type rearrangement and i-cleavage (Wang et al., 2022). Therefore whole fragmentation pattern (Scheme 1) is characteristic of lasiocarpine (**1**), a common compound previously isolated from *H. europaeum* (Shimshoni et al., 2021). Literature review revealed that lasiocarpine (**1**), possess cytotoxicity against HepaRG cells, human (caucasian) hepatocytes and corrected human (Chinese) hepatocytes (Al-Snafi, 2018).

The third node (Fig. 3) appeared at m/z 395.2338, attested for molecular formula $C_{21}H_{33}NO_6$, while fragment ions at m/z 220.1339 $[C_{13}H_{18}NO_2]^+$ and at m/z 120.0809 $[C_8H_{10}N]^+$ produced by the loss of ester linkage $[M^+-C_5H_7O_2]$, with the loss of 100 Da.

Similar behavior was observed for a node (Fig. 3) at m/z 413.2413 with molecular formula $C_{21}H_{35}NO_7$. A similar fragmentation pattern was also observed with characteristic fragments at m/z 338.1975 $[C_{18}H_{28}NO_5]^+$ and 222.1498 $[C_{13}H_{20}NO_2]^+$. These fragments differ by 2 Da from fragment ions of compound **1**, suggesting **2** as a derivative of **1** with a double bond either in ring system or in the chain ester linkages. The fragment ions pattern as shown in scheme 1 indicated that the double bond was present at C-7 part of ester linkage as the loss of m/z 101.05 $[C_5H_9O_2]^+$ fragment ion confirmed the presence of double bond at C-7. As the *in silico* predictor was unable to find the structural hit for this node, compound **2** was assumed to be a new analogue of lasiocarpine (**1**). The proposed biosynthetic link of the known and new compound is given in Scheme 1. The third node (Fig. 3) appeared at m/z 395.2338, attested for molecular formula $C_{21}H_{33}NO_6$, while fragment ions at m/z 220.1339 $[C_{13}H_{18}NO_2]^+$ and at m/z 120.0809 $[C_8H_{10}N]^+$ produced by the loss of ester linkage $[M^+-C_5H_7O_2]$, with the loss of 100 Da. This fragmentation pattern is also similar to that of compound **1** but with 16 Da difference in molecular mass, showing it as a derivative of **1** with an OH group less in compound **3**. This compound was identified as 5-deoxylasiocarpine (**3**), previously isolated from other *Heliotropium* species (Ning et al., 2019). Since compound **3** is also a derivative of **1** (Scheme 1), therefore, both of them
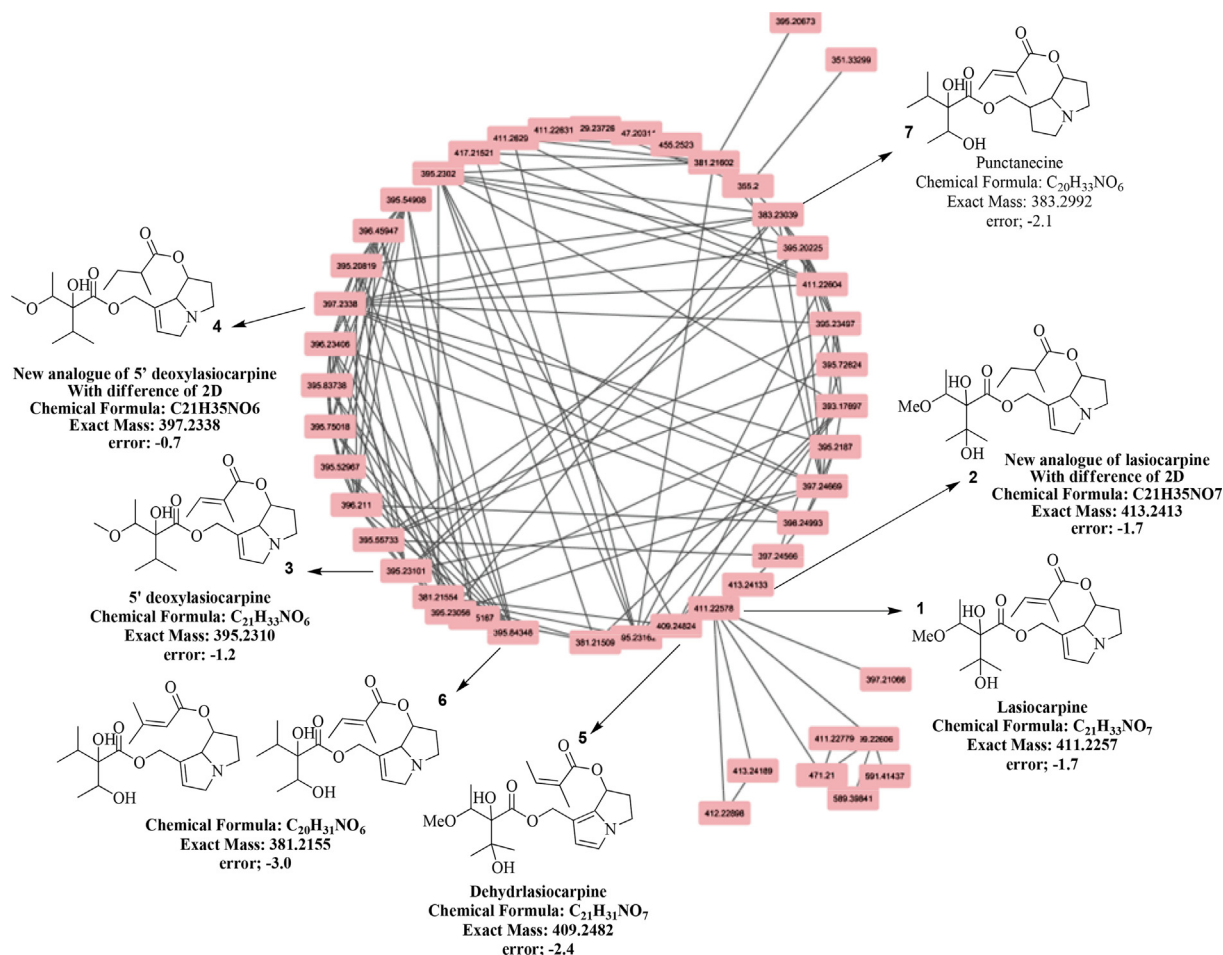
Fig. 3 Cluster 4 indicating the Pyrrolizidine alkaloids with their molecular formula, exact mass and error in ppm.
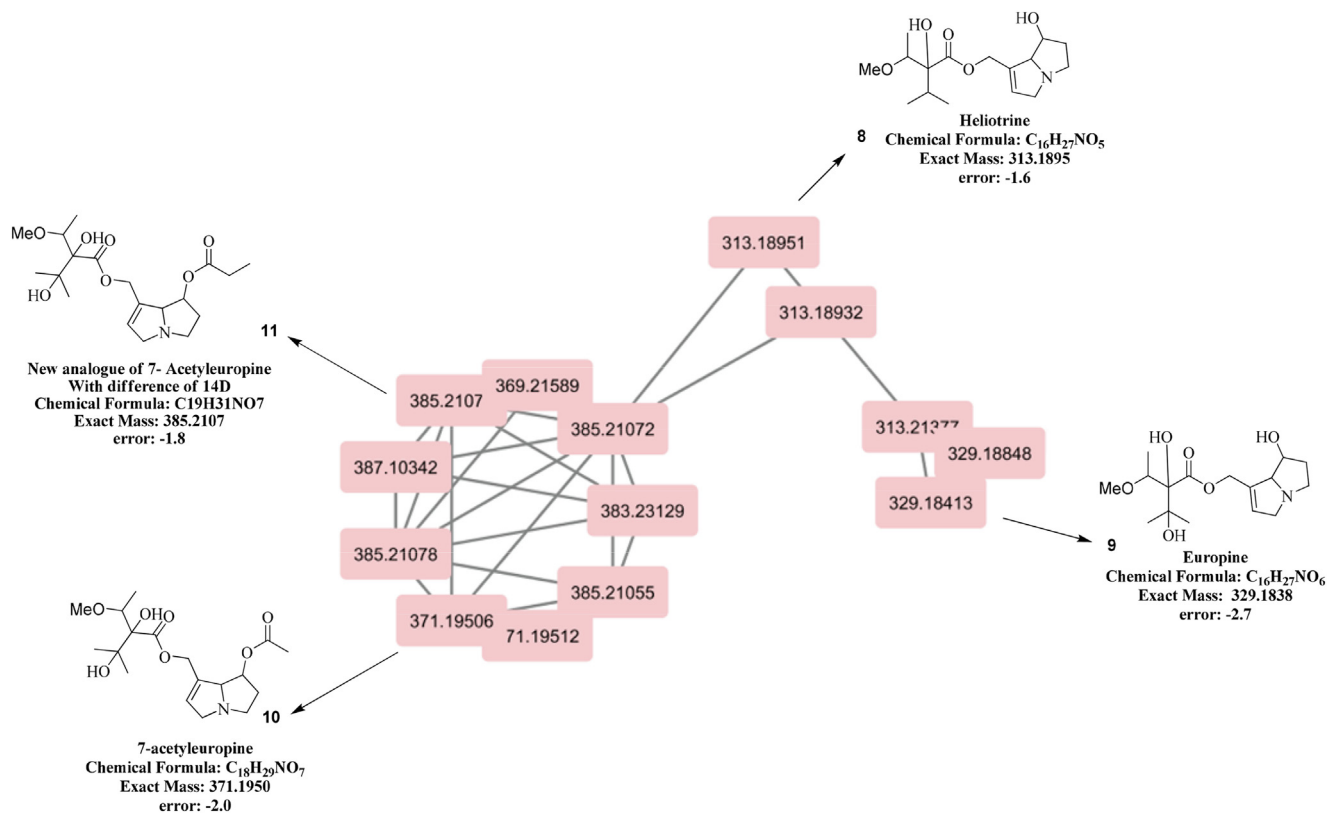
Fig. 4 Cluster 18 indicating the Pyrrolizidine alkaloids with their molecular formula, exact mass and error in ppm.
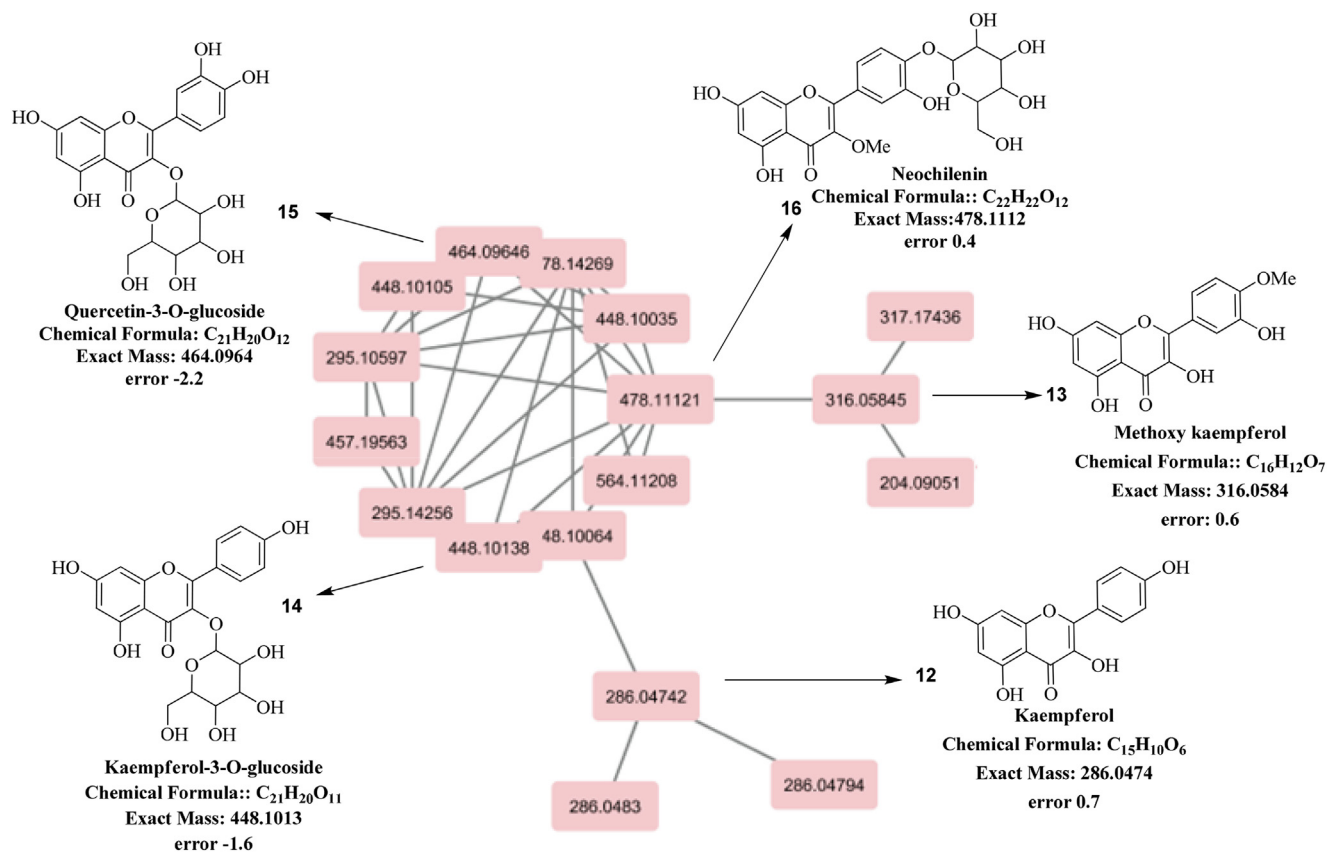
Fig. 5 Cluster 19 indicating the flavonoid glycosides with their molecular formula, exact mass and error in ppm in negative mode.

Table 3 Binding energies of docked confirmations of known and new compounds identified form *Heliotropium dasycarpum*.

Sr. No.	Compound name	Docking scores Kcal/mol
1	Lasiocarpine (**1**)	−4.46
2	New analogue of lasiocarpine (**2**)	−4.24
3	5′-deoxylasiocarpine (**3**)	−5.18
4	New analogue of 5′-deoxylasiocarpine (**4**)	−4.34
5	Punctanecine (**7**)	−5.38
6	Heliotrine (**8**)	−4.41
7	7- Acetyleuropine (**10**)	−4.26
8	New analogue of 7-Acetyleuropine (**11**)	−4.94
9	Quercetin-3-O-glucoside (**15**)	−5.44
10	Neochilenin (**16**)	−4.30
Standard	Thiourea	−3.19

tend to occur in the same cluster providing the evidence of success of MN based dereplication.

The next node (Fig. 3) at m/z 397.2067, corresponding to the molecular formula as $C_{21}H_{35}NO_6$, found fit for compound **4**, since it showed similar fragmentation pattern to that in spectra of compound **3** with a 2 Da difference. As other fragment ions at m/z 220.1339 and 120.0809 were similar to those in spectrum of compound **3**, it suggested reduction of C-7 ester linkage double bond in compound **4**. Absence of any hit in Sirius+ CSI:FingerID database prompted to conclude compound **4** as a new analogue of 5-deoxylasicarpine (**3**). Scheme 1 describes the biosynthetic pathway of the new compound formation from the known 5-deoxylasicarpine which in turn is derivative of lasiocarpine (**1**).

Analysis of another node at m/z 409.2482 led to the identification of compound **5**, with molecular formula $C_{21}H_{31}NO_7$. Since its fragmentation data was also similar to that of compound **1** (Table 2) with difference of 2 Da, showing one additional double bond in compound **5**. Based on the fragment ions, the additional double bond could be placed in the ring system (Scheme 1). Comparing mass fragments with the published literature, this node was identified as dehydrolasiocarpine (**5**), which is reported to induce hepatotoxicity and genotoxicity and tumor by binding to cellular protein and DNA (Shafiei et al., 2002).

The node at m/z 381.2155 (Fig. 3) afforded molecular formula $C_{20}H_{31}NO_6$ with fragment ions similar to necine unit and due to breakage of ester linkage (m/z 120.0808 and 220.1710 respectively) resulted in the identification of for com-

pound **6**. Whole fragmentation pattern was almost similar to that of compound **3** with 14 Da difference in molecular mass. Thus compound **6** could be characterized as a derivative of **3** with a less methyl group in **6**. Since the identification of structure by *in silico* predictor is not always complete with only MS, two potential structures (symviridine or symphytine) for compound **6** were assigned to this precursor ion, however, none of these two compounds were identified previously from any *Heliotropium* species (Zhao et al., 2011). Literature review showed that structural analogues symviridine and symphytine of compound **6**, being toxic compounds cause veno-occlusive liver disease (Roeder et al., 1992).

Next node at m/z 383.2992 was attested with formula $C_{20}H_{33}NO_6$ for compound **7**. The fragment ions were found same (m/z 220.1367 and 120.0810) as were seen for compound **6** but with difference of 2 Da, indicating mass of compound **7** ascends due to reduction of a double bond in the ring. Literature search revealed it as known compound punctanecine (**7**) (Mandić et al., 2015). This compound has also been reported for the first time from *H. dasycarpum*. In general, cluster 4 (Fig. 3) was predicted to contain diesters of pyrrolizidine alkaloids.

Fragmentation behavior of MS/MS data of cluster 18 (Fig. 4) revealed it to be mono- and diesters of pyrrolizidine alkaloids too with the basic skeleton of necine base (Fig. 2) with fragment ion of $[M+H-156]^+$. Node ate m/z 313.1895 depicted the molecular formula $C_{16}H_{27}NO_5$ with usual fragments of necine base at m/z 156.1021 and 138.0914 representing heliotrine (**8**), a common compound of this genus (Ning et al., 2019). Fragmentation pattern of another node (Fig. 4) at m/z 329.1841, with molecular formula $C_{16}H_{27}NO_6$ for compound **9** was also found similar to that of compound **8**, it displayed characteristic ions at m/z 254.1394, 156.1024 and 138.0916 (Table 2) as were seen for compound **8**. Its mass difference (16 Da) with compound **8** can be corresponded to additional OH group in **9**. Therefore, based on the observed fragmentation pattern (Scheme 2) and its comparison with literature values, it was identified as europine (**9**) (Roeder et al., 2015). In literature review, europine (**9**) displayed antifungal and insect antifeedant activity (Reina et al., 1995). For the next node (Fig. 4) at m/z 371.1950, offered molecular formula $C_{18}H_{29}NO_7$ for compound **10**. Its fragments at m/z 312.1816, obtained by the loss of 59 Da (M^+-$C_2H_3O_2$), 154.0865 and 136.0760 were characteristic of a known compound 7-acetyleuropine (**10**). Compound **11** (node at m/z 385.2101, with molecular formula as $C_{19}H_{31}NO_7$) was presumed as analogue of 7-acetyleuropine (**10**) due to similarity in fragments with difference of 14 Da suggesting it a derivative with an additional

Table 4 Binding free energies of best docked compounds identified form *Heliotropium dasycarpum*, with Urease enzyme.

Sr. no	Compound Name	Docking scores (Kcal/mol)	Hydrophobic interactions	Hydrogen Bonds	Other Interactions
1	5′-deoxylasiocarpine (**3**)	−5.18	Met588, Asp587, Val591, Gln 635 & Arg439	–	–
2	Punctanecine (**7**)	−5.38	Ser 421, Ser422, Thr715, Lys716, Pro717, Asp730, Lys745, Met 746, Phe838 & Leu839	Lys 716 & Leu839	Ionic bond Asp730
3	Quercetin-3-O-glucoside (**15**)	−5.44	Glu418, Ser421, Ser422, Thr715, Lys 716 & Phe838	Glu418, Ser421, Thr715 &Leu839	Cation π; Interaction Lys 716

CH$_2$ group (propionyloxy group) at C-7 ester linkage as depicted in scheme 1. Since no structural hits appeared in database for this node, thus compound **11** was identified as a new metabolite.

Structural annotation of cluster number 19 (Fig. 5) showed the typical fragmentation pattern for flavonoids and flavonoid-O-glycosides (negative ionization mode). Node at m/z 286.0553, attested for the molecular formula as C$_{15}$H$_{10}$O$_6$, was identified as a flavonol with characteristic cleavage of flavone moiety giving fragment ion at [M-152]$^+$. This fragmentation pattern, in comparison with literature confirmed it to be kaempferol (**12**), an important known phytochemical (March and Miao, 2004). Similarly, node at m/z 316.0583 with formula as C$_{16}$H$_{12}$O$_7$ was predicted as methoxy kaempferol derivative (**13**), with fragment at m/z 302.0431 [M-CH$_2$]$^+$, will be more

probably the loss of methyl group 15 Da-CH$_3$ group, and fragment at m/z 285.0404 due to loss of methoxyl moiety. (negative ionization mode).

The node at m/z 448.1006 was identified as 3-O-glycoside of kaempferol (**14**) due to characteristic fragment at m/z 287.0577 of flavone skeleton and another characteristic fragment at m/z 163.0623 for sugar moiety, usually observed in mass spectra of 3-O-glycoside derivative (Figueirinha et al., 2008) in negative mode. Tracking down the next node (Fig. 5) at m/z 464.0955, which had 16D higher mass than compound **14** was attested for the molecular formula C$_{21}$H$_{20}$O$_{12}$. Other characteristic fragment ions at m/z 303.0508 (flavonol moiety) and 163.0623 (hexose part) indicated it to be 3-O-glycoside derivative of quercetin (**15**). Next node at m/z 478.1111 depicted the molecular formula as C$_{22}$H$_{22}$O$_{12}$, could be identified as 3-O-

A) 5' deoxylasiocarpine-Urease Complex

B) Punctanecine-Urease Complex

C) Quercetin-3-O-glucoside-Urease Complex
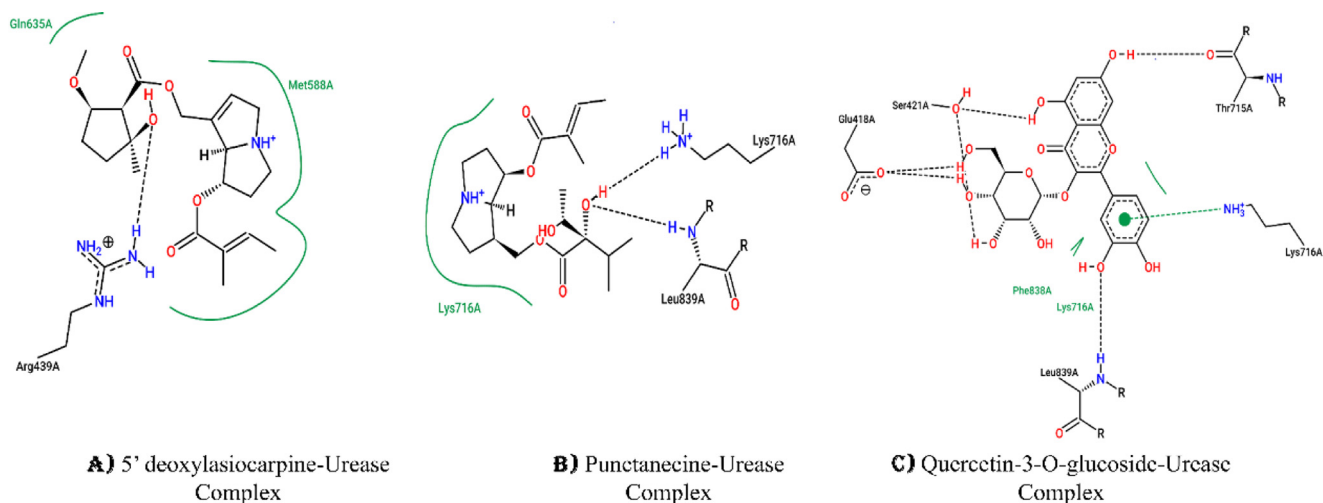
Fig. 6 2D Interaction diagrams generated through PoseView **A)** 5' deoxylasiocarpine showing hydrophobic interaction with Met588 and Gln635 of Urease and hydrogen bond with Arg439. **B)** Punctanecine showing hydrophobic interactions with Lys716 and hydrogen bonding with Lysine716 and Leu839 of Urease. **C)** Quercetin-3-O-glucoside showing hydrophobic interaction with Lys716 and Phe838, while hydrogen bonds were mediated with Glu418, Ser421, Thr715, Lys716 and Leu839.

A) 5' deoxylasiocarpine-Urease Complex

B) Punctanecine-Urease Complex

C) Quercetin-3-O-glucoside-Urease Complex
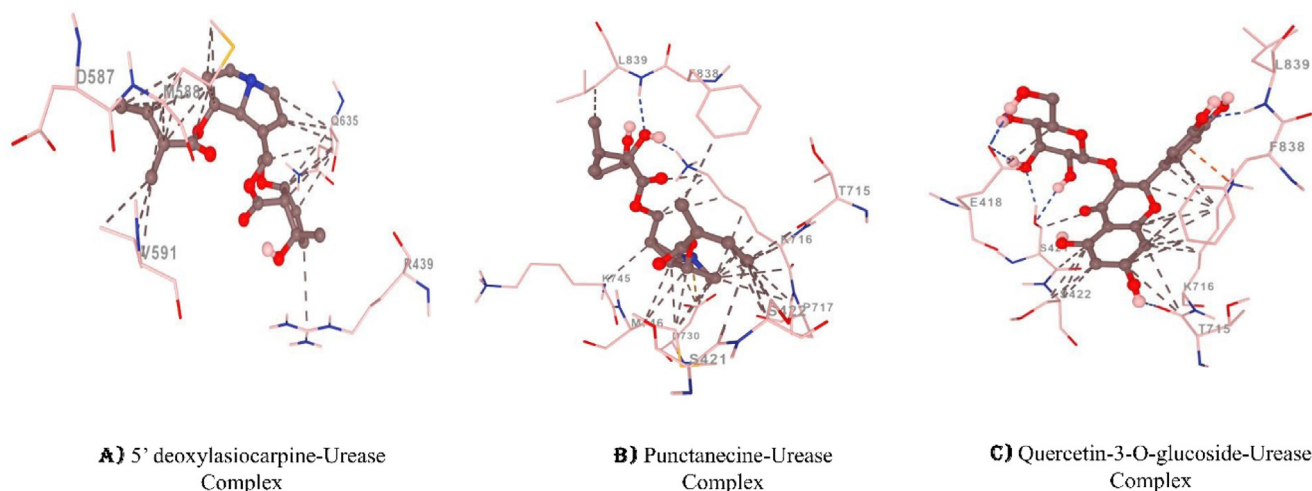
Fig. 7 (A-C) 3D interaction diagrams of (A) 5' deoxylasiocarpine, (B) Punctanecine and (C)Quercetin-3-O- glucoside generated through ezCADD. Blue dotted lines indicate hydrogen bonds, grey dotted lines indicates hydrophobic interaction, orange dotted lines indicate cation pi interaction and yellow dotted lines indicate ionic bonds.

Table 5 Analysis of compounds identified form *Heliotropium dasycarpum* using FAF*Drugs*4 for ADME/Tox properties.

ID	Parameters Standards	Lasiocarpine (1)	New analogue of lasiocarpine (2)	5′ deoxy-lasiocarpine (3)	New analogue of 5′deoxy lasiocapine (4)	Punctanecine (7)	Heliotrine (8)	Acetyl-europine (10)	New analogue of Acetyleuropine (11)	Quercetin-3-O-glucoside (15)	Neochilenin (16)
MW	100.0–600.0	411.49	413.52	395.49	397.52	383.48	313.39	371.43	385.47	464.38	478.42
logP	−3.0–6.0	1.28	1.52	2.27	2.28	2.18	0.91	0.08	0.65	0.36	0.22
tPSA	≤ 11	106.73	106.73	86.5	86.5	97.5	80.43	106.73	95.73	210.18	195.6
Rotatable bond	≤ 11	10	11	9	11	9	7	9	10	4	5
Rigid bond	≤ 30	12	11	16	11	12	10	11	11	24	24
HBD	≤ 7	2	2	1	1	2	2	2	1	8	7
HBA	≤ 12	8	8	7	7	7	6	8	8	12	12
Rings	≤ 6	1	1	2	1	1	1	1	1	3	3
Max. size ring	≤ 18	8	8	8	8	8	8	8	8	10	10
Num charges	≤ 4	1	1	1	1	1	1	1	1	0	0
Total charge	−8	1	1	1	1	1	1	1	1	0	0
Carbon atoms	3–35	21	21	21	21	20	16	18	19	21	22
Hetero atoms	1–15	8	8	7	7	7	6	8	8	12	12
ratio H/C	0.1–1.1	0.38	0.38	0.33	0.33	0.35	0.38	0.44	0.42	0.57	0.55
Lipinski violation		0	0	0	0	0	0	0	0	2	2
Solubility (mg/l)		32529.57	29420.83	17322.19	19352.74	19150.23	47140.5	75046.71	52869.8	25415.67	29795.53
Solubility Forecast Index		Good Solubility	Good Solubility	Good Solubility	Good Solubility	Good Solubility	Good Solubility	Good Solubility	Good Solubility	Good Solubility	Good Solubility
Oral bioavailability VEBER		Good	Good	Good	Good	Good	Good	Good	Good	Good	Good
Oral Bioavailability EGAN		Good	Good	Good	Good	Good	Good	Good	Good	Good	Good
Stereo centers		5	7	8	7	6	5	5	6	5	7
Result		Accepted	Accepted	Accepted	Accepted	Accepted	Accepted	Accepted	Accepted	Accepted	Accepted

methyl glycoside derivative of quercetin (**16**), due to 14 Da difference with that of compound **15**. The base peak at *m/z* 285.1241 and fragment ion due to hexose moiety substantiated the deduction of compound **16** to be methyl ether of quercetin 3-O-glycoside (Myagchilov et al., 2020), (Iwashina et al., 1984).

3.4. Anti-urease docking studies and ADME/Tox screening of identified compounds

MN base Dereplication strategy has helped in documentation of pyrrolizidine alkaloids, flavonoids and flavonoid glycosides. The pyrrolizidine alkaloids including three new analogues were docked to validate the urease inhibitory activity of these compounds. The drug-likeliness of these compounds was also assessed for their potential as future drugs leads. Compounds **1–4**, **7**, **8**, **10**, **11**, **15** and **16** were docked against urease enzyme comparing with standard thiourea. The binding energies of inhibitors and compounds are given in Table 3. All the compounds have better binding energies as compared to thiourea (-3.19 Kcal/mol). The compounds, 5′-deoxylasiocarpine (**3**), punctanecine (**7**) and quercetin-3-O-glucoside (**15**) showed better binding energies with values of −5.18, −5.38 and −5.44 Kcal/mol respectively. Compound **3** made several hydrophobic interactions with the urease, while **7** showed two hydrogen bonds with Lys716 and Leu839 along with an ionic interaction between nitrogen and Asp730 and

multiple hydrophobic interactions. Quercetin-3-O-glucoside (**15**) showed seven hydrogen bonds (Thr715, Ser421, Ser421, Glu418, Glu418, Glu418, Leu839) along with one cationic π interaction (Lys716) and multiple hydrophobic interactions making its binding energy −5.44 kcal/mol. The binding interactions of these compounds along with binding energies are given in Table 4. The 2D binding interactions of compounds **3**, **7** and **15** are shown in Fig. 6 (A-C). Pose View generated the 2D interactions. The binding energy for thiourea was calculated to be −3.19 kcal/mol which is comparable to binding energy reported in literature.[13] The 3D interaction of thiourea within active site was visualized using UCSF Chimera (Fig. 8) (Pettersen et al., 2004). The ezCADD was used for building 3D binding interaction of these three compounds (Fig. 7).

3.5. ADME/Tox screening of the compounds (**1–4, 7, 8, 10, 11, 15 and 16**)

All the compounds follow the standardized parameters of FAF*Drugs*4 and follow Lipinski's rule. The results suggest that these compounds can act as potential drugs, however, their toxic properties need to be studied. LogP values indicate towards oral bioavailability, H-bond acceptors and donors of the tested compounds. Furthermore, good permeability of evaluated compounds through plasma membrane is taken into account through topological polar surface (tPSA). The results of ADME/Tox analysis are shown in Table 5.

Fig. 8 Binding interaction of Thiourea (brown) within active site of Urease (sky blue). Nickel atoms are shown in green color. Two hydrogen bonds with bond distance 1.994 Å and 2.058 Å are shown with dark blue solid lines with residue Ser497(violet red) of protein.

3.6. Density functional theory study descriptors

The molecular reactivity and structure of organic compounds can be perfectly described and interpreted with help of DFT which is a universal computer aided technique in order to discover their quantitative structure activity affiliation by utilization of different quantum chemical and geometrical descriptors (Horchani et al., 2020). Examination of electronic characters of molecules as a result of DFT studies plays main part to uncover the pharmacological features of organic molecules (Parveen et al., 2020).

3.6.1. Frontier molecular orbital (FMO) analysis

In a molecule the most imperative orbitals are HOMO and LUMO as they play a significant part in exploring the electrical and optical features as well as the quantum chemistry of compounds (Fleming, 1977). The HOMO (highest occupied molecular orbital) and LUMO (lowest occupied molecular orbital) are collectively known as frontier molecular orbitals (FMO) (Fig. 9) and are associated with ionization potential and electron affinity of molecule, respectively.

The E_{HOMO} (energy of HOMO) typifies the capability of a molecule to donate electron, whereas E_{LUMO} (energy of LUMO) governs electron accepting ability. So, higher E_{HOMO} values signposts a better propensity towards the electron donation. Ensuing in good biological potential related with increasing E_{Homo} value (Bendjeddou et al., 2016). Activity rankings of under studied molecules according to (Table 6) with increasing E_{Homo} values is as follows:

(3) > (1) > (7) > (8) > (2) = (4) > (11) > (10) > (16) > (15)

However, the activity ranking of compounds on basis of E_{LUMO} is as follows:

(2) > (11) > (4) > (10) > (8) > (1) > (3) > (7) > (16) > (15)

The energy gap (ΔE) between E_{Homo} and E_{LUMO} is very significant as it signposts the chemical reactivity of molecule. A small value of ΔE indicates that the molecule is more reactive and softer while large value of ΔE is an indication that molecule is more stable, less reactive and hard (de Oliveira et al., 2020; Rahman et al., 2020). Among the studied compound, (15) is most reactive, softest and least hard molecule with lowest ΔE (0.1361 eV) value, lowest chemical hardness

E_{LUMO} (eV) = -0.0602 ΔE = 0.1509 E_{HOMO} (eV) = -0.2112

E_{LUMO} (eV) = -0.0298 ΔE = 0.1835 E_{HOMO} (eV) = -0.2134

E_{LUMO} (eV) = -0.0277 ΔE = 0.1912 E_{HOMO} (eV) = -0.2190

Punctanecine (7)   Heliotrine (8)   7- Acetyleuropine (10)

E_{LUMO} (eV) = -0.0244 ΔE = 0.1914 E_{HOMO} (eV) = -0.2159

E_{LUMO} (eV) = -0.0998 ΔE = 0.1361 E_{HOMO} (eV) = -0.2359

E_{LUMO} (eV) = -0.0832 ΔE = 0.1417 E_{HOMO} (eV) = -0.2249

New analogue of 7- Acetyleuropine (11)   Quercetin-3-O-glucoside (15)   Neochilenin (16)
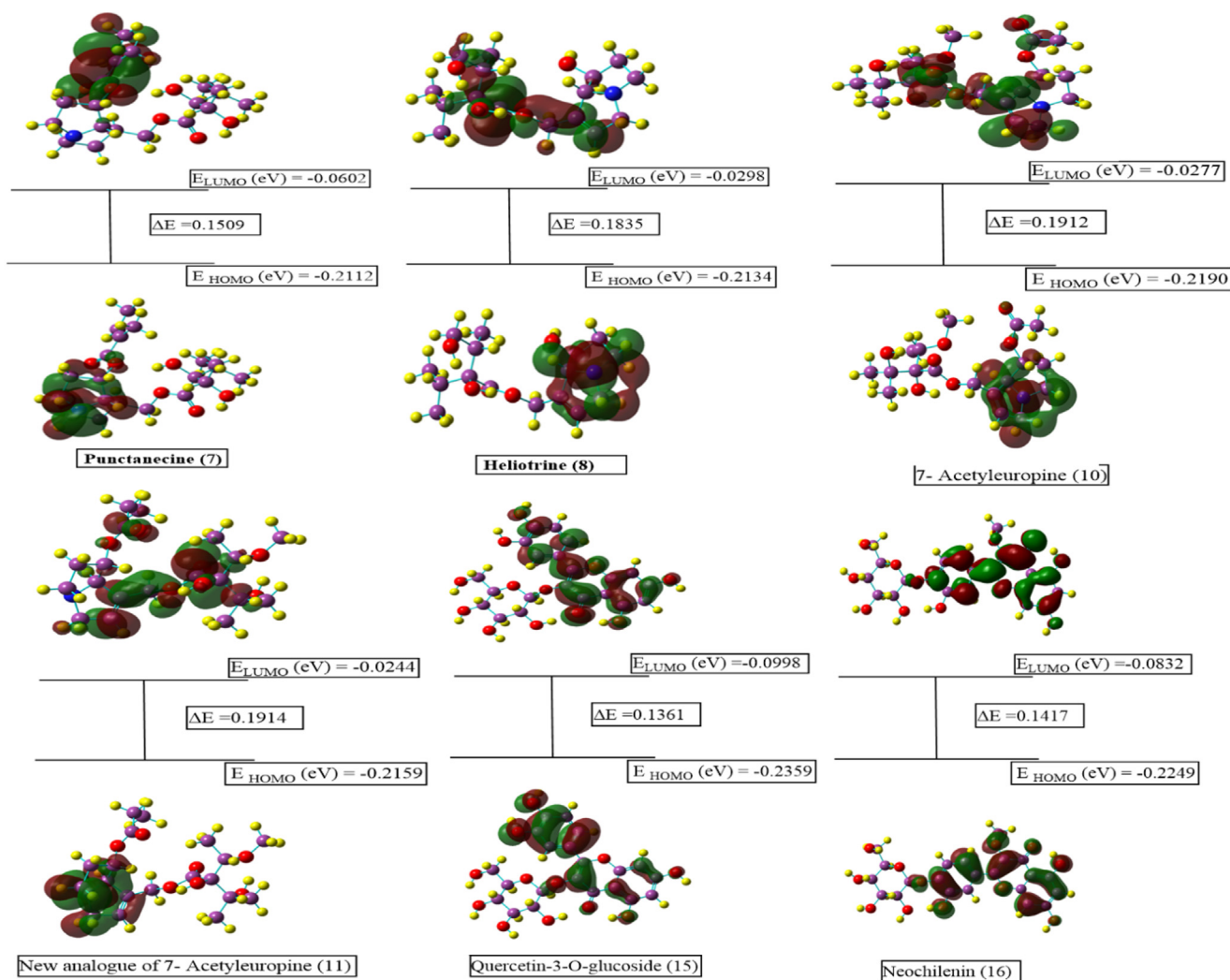
Fig. 9 Contour diagrams of FMOs comprising the highest occupied molecular orbitals (HOMO) and the lowest unoccupied molecular orbitals (LUMO) along with energy gap.

Table 6 Quantum and geometrical based computational parameters based on DFT calculations having 321-G basis set for the in order to facilitate SAR studies of compounds, where E_{HOMO} (eV), E_{LUMO} (eV), Energy Gap "$\Delta E = E_{LUMO} - E_{HOMO}$ (eV)", Dipole Moment "μ(Debye)", Global Hardness "η (eV)", Electronegativity "χ (eV)", Chemical Potential "CP", Nucleophilicity Index "N", Electrophilicity Index "(ω)", Ionization Potential "$I = -E_{HOMO}$ (eV)", Electronic Energy "E (Hatree)", global softness "(S)", additional electronic charges "(ΔNmax).

Sr. No.	Compounds	Parameters													
		E_{LUMO} (eV)	E_{HOMO} (eV)	ΔE (eV)	A (eV)	I (eV)	χ (eV)	μ (eV)	η (eV)	S	ω (eV)	N	ΔN_{max} (eV)	d.p D	E Hartree
1	Lasiocarpine (1)	0.0483	0.2085	0.1602	0.0483	0.2085	0.1284	0.1284	0.0801	6.24	0.1029	9.717	1.603	3.7250	1401.325
2	New analogue of lasiocarpine (2)	0.0239	0.2141	0.1902	0.0239	0.2141	0.1190	0.1190	0.0951	5.25	0.0744	13.43	1.251	5.4921	1402.548
3	5′deoxylasiocarpine (3)	0.0495	0.2057	0.15619	0.0495	0.2057	0.1276	0.1276	0.0781	6.40	0.1043	9.584	1.634	0.76401	1326.102
4	New analogue of 5′deoxylasiocarpine (4)	0.0258	0.2141	0.1883	0.0258	0.2141	0.1199	0.1199	0.0941	5.31	0.1529	6.540	1.274	3.0864	1327.329
5	Punctanecine (7)	0.0602	0.2112	0.1509	0.0602	0.2112	0.1357	0.1357	0.0754	6.62	0.1237	8.079	1.797	4.8794	1288.027
6	Heliotrine (8)	0.0298	0.2134	0.1835	0.0298	0.2134	0.1216	0.1216	0.0917	5.44	0.0806	12.40	1.325	7.2157	1056.743
7	7- Acetyleuropine (10)	0.0277	0.2190	0.1912	0.0277	0.2190	0.1236	0.1236	0.0956	5.22	0.0796	12.56	1.290	8.2019	1284.594
8	New analogue of 7- Acetyleuropine (11)	0.0244	0.2159	0.1914	0.0244	0.2159	0.1202	0.1202	0.0957	5.22	0.0753	13.28	1.255	2.5157	1323.916
9	Quercetin-3-O-glucoside (15)	0.0998	0.2359	0.1361	0.0998	0.2359	0.1679	0.1679	0.0680	7.34	0.2071	4.827	2.467	7.1707	1714.863
10	Neochilenin (16)	0.0832	0.2249	0.1417	0.0832	0.2249	0.1541	0.1541	0.0709	7.05	0.1674	5.971	2.174	8.9873	1754.158

(η = 0.0680) and highest softness (S = 7.34). Consistent with Table 6. increase in reactivity order of molecules is as follow:

(**15**) > (16) > (**7**) > (**3**) > (**1**) > (**8**) > (**4**) > (**2**) > 10) > (**11**)

3.6.2. Global reactivity parameters

Chemical potential (μ), electronegativity (χ), chemical hardness (η), softness (S), electronic energy (E), electrophilicity index (ω), nucleophilicity Index (N), ionization potential (I), Electronic Charges (ΔN_{max}) and dipole moment are the global parameters to assess the chemical reactivity of a molecule (Zarren et al., 2021).

Larger value of electronegativity (χ) and electrophilicity index (ω) indicate the good electron accepting ability of a molecule. So, compound (**15**) is considered best electrophile

with highest (χ) and (ω) values, −0.1679 eV and 0.2071 eV, respectively (Abbaz et al., 2019). A compound with higher nucleophilicity index (N) value and lower electrophilicity (ω) value offers good biological potential. has lowest electrophilicity and highest nucleophilicity index. Compound (**2**) is considered to have excellent biological potential with highest nucleophilicity index (N = 13.43) and lowest electrophilicity (ω = 0.0744) values (Table 6).

Charge densities in a compound and its bond properties can be measured by dipole moment. Fig. 10 displayed the vector of the dipole moment of all the under studied molecules. Compound (**16**) has large dipole moment value as compared to other compounds that revealed that (**16**) has the finest charge distribution and well-adjusted bond distance. This symbolizes that compound (**16**) exhibited the paramount conductivity
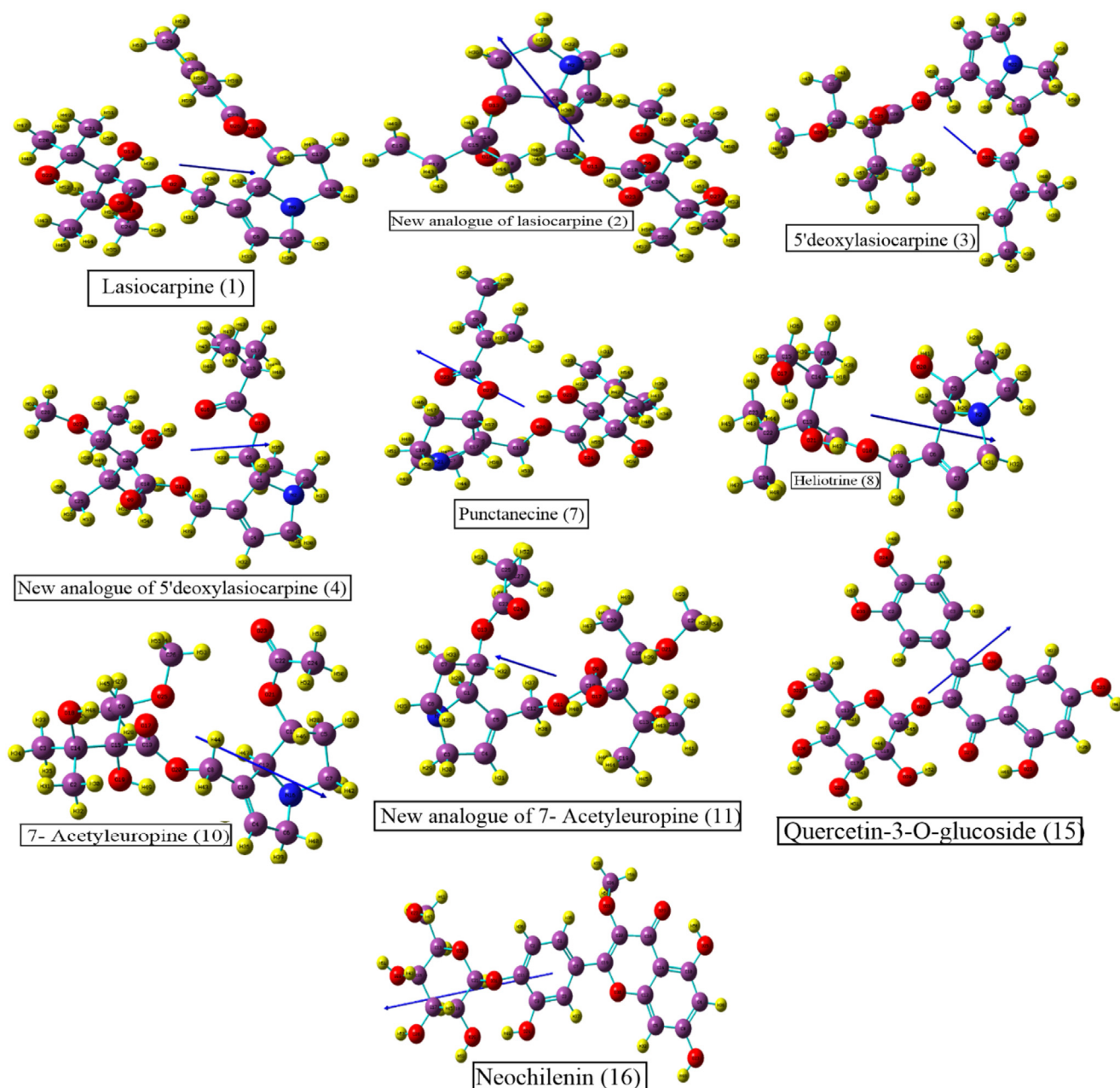
Fig. 10   The vector of the dipole moment of all the under studied molecules.

upgraded by oxidation (Ajeel et al., 2015; Ahmed et al., 2017; Sayin and Üngördü 2018). On the basis of highest negative value of Electronic Energy (E), compound (16) is most sable compound among all discussed compounds.

3.6.3. Molecular electrostatic potential (MEP)

The MEP visuals allows us to foresee variably charged zones of a molecule which is valuable to forecast how molecules may react to each other, nature of chemical bonds and detection of location of nucleophilic and electrophilic attack (Valarmathi et al., 2021). The computed electrostatic potential as well as predicted sites for electrophilic and nucleophilic attack through MEP map for all studied compounds are shown in Fig. 11. The blue to red color of the diagrams suggests the electron-poor to electron-rich areas (Parveen et al., 2022). The position of attack of nucleophile is indicatable by blue color that is dispersed mainly around hydrogen atoms, presenting its competence to react with a nucleophile.
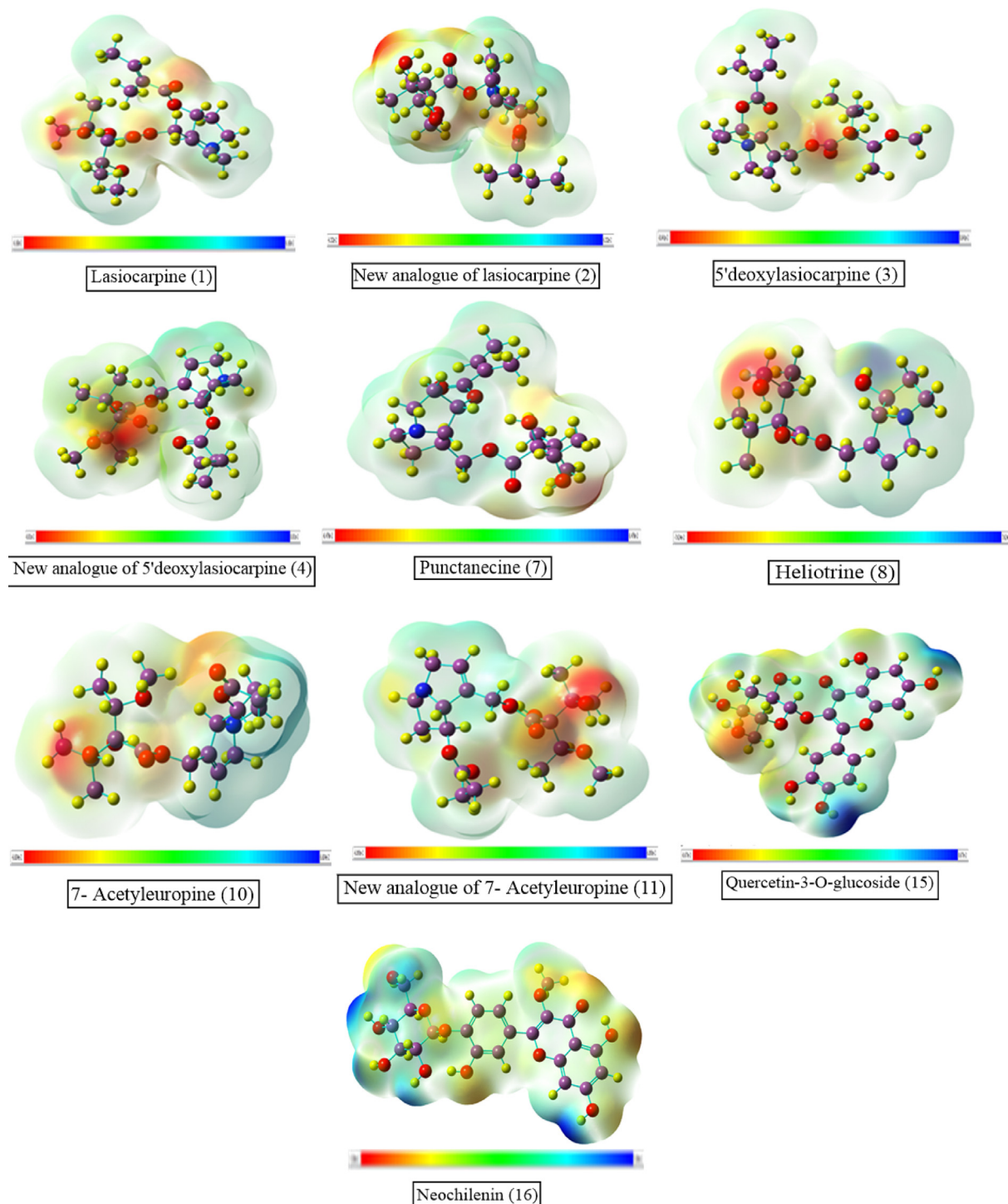
Fig. 11 MEP of the compounds based on SCF energy.

However, yellow or red coloration is a suggestion of position of attack of an electrophile which is noticeably appeared nearby the oxygen atoms thus all the oxygen atoms have the competence to react with electrophiles. While the region with green coloration signifies the area of neutral reactivity.

4. Conclusion

Heliotropium dasycarpum, being important component of folk medicinal system, was investigated for its Biomedical potential. Although methanolic extract (HdM) and its fractions (HdH, HdE and HdW) were inactive in anticancer assay and were weakly immunomodulators; but ethyl acetate fraction (HdE) potentially inhibited the activity of urease enzyme. Chemical profiling through HR-LCMS/MS of HdE disclosed the presence of 08 known (**1**, **3**, **5–11**) and three new (**2**, **4** and **11**) pyrrolizidine alkaloids, along with and five known flavonoid-derivatives (**12–16**). Most of these known compounds are already reported as cytotoxic or potent antioxidant. Docking studies of compounds **3**, **7** and **15** indicated potential inhibitory activity against urease enzyme as these compounds made special hydrophobic interactions with the urease enzyme while ADME/Tox analysis also indicates that the compounds have drug-like properties and hence validated antiurease activity of HdE, which can serve as potential drugs for future use. These studies suggested the ethyl acetate soluble fraction of crude methanolic extract of *Heliotropium dasycarpum* may be considered as important component of herbal drug against infection stones, pyelonephritis, peptic ulceration and hepatic encephalopathy, or may serve to provide pure metabolites for such drug development.

Declaration of Competing Interest

The authors declare that they have no known competing financial interests or personal relationships that could have appeared to influence the work reported in this paper.

Acknowledgements

Appendix A. Supplementary material

Supplementary data to this article can be found online at https://doi.org/10.1016/j.arabjc.2023.104655.

References

Abbaz, T., Bendjeddou, A., Villemin, D., 2019. Density functional theory studies on molecular structure and electronic properties of sulfanilamide, sulfathiazole, E7070 and furosemide molecules. J. Appl. Chem. 12, 60–69.

Achakzai, J.K., Panezai, M.A., Akhtar, B., et al., 2020. In vitro anti-inflammatory, anticancer (MCF-7, 3T3, and HeLa Cell Lines), and Brine Shrimp Lethality Assay and FTIR analysis of the extract and fractions of the whole plant of Heliotropium europaeum. Mediators of Inflammation. 2020.

Ahmad, S., Ullah, F., Zeb, A., et al, 2016. Evaluation of Rumex hastatus D. Don for cytotoxic potential against HeLa and NIH/3T3 cell lines: chemical characterization of chloroform fraction and identification of bioactive compounds. BMC Complement. Altern. Med. 16, 308. https://doi.org/10.1186/s12906-016-1302-y.

Ahmed, M.N., Yasin, K.A., Hameed, S., et al, 2017. Synthesis, structural studies and biological activities of three new 2-(pentadecylthio)-5-aryl-1, 3, 4-oxadiazoles. J. Mol. Struct. 1129, 50–59.

Ajeel, F.N., Khudhair, A.M., Mohammed, A.A., 2015. Density functional theory investigation of the physical properties of dicyano pyridazine molecules. Int. J. Sci. Res. 4, 2334–2339.

Al-Snafi, A., 2018. Pharmacological and toxicological effects of Heliotropium undulatum [h. Bacciferum] and Heliotropium europaeum-a review. https://doi.org/10.5281/zenodo.1214982.

Aman, H., Rashid, N., Ashraf, Z., et al, 2020. Synthesis, density functional theory (DFT) studies and urease inhibition activity of chiral benzimidazoles. Heliyon. 6, e05187.

Bendjeddou, A., Abbaz, T., Gouasmia, A., et al., 2016. Molecular structure, HOMO-LUMO, MEP and Fukui function analysis of some TTF-donor substituted molecules using DFT (B3LYP) calculations. 1–9.

Chen, L., Mulder, P.P., Peijnenburg, A., et al, 2019. Risk assessment of intake of pyrrolizidine alkaloids from herbal teas and medicines following realistic exposure scenarios. Food Chem. Toxicol. 130, 142–153.

Chen, T., Mei, N., Fu, P.P., 2010. Genotoxicity of pyrrolizidine alkaloids. J. Appl. Toxicol.: Int. J. 30, 183–196.

Chiesa, L.M., Panseri, S., Nobile, M., et al., 2018. Distribution of POPs, pesticides and antibiotic residues in organic honeys from different production areas Part A Chemistry, analysis, control, exposure & risk assessment.

de Oliveira, V.M., Estácio, S.P., da Silva Mendes, F.R., et al, 2020. Characterization of rotenoid stemonal by semiempirical methods and molecular docking. SN Appl. Sci. 2, 1–8.

Demıray, H., Gemıcı, M., Karabey, F., 2013. Chemical constituents of Heliotropium hirsututissimum Grauer (Heliotrope)(Sigil otu, Bambil)(Sonnenwende) and ecotype. Asian J. Chem. 25, 3725–3730.

Fayed, M.A., 2021. Heliotropium; a genus rich in pyrrolizidine alkaloids: A systematic review following its Phytochemistry and Pharmacology. Phytomedicine Plus. 100036.

Figueirinha, A.P., P. r.-A. JJ., S.-B. C., et al., 2008. Cymbopogon citratus leaves: Characterization of flavonoids by HPLC-PDA-ESI/MS/MS and an approach to their potential as a source of bioactive polyphenols. Food Chem. 110, 718–728.

Fleming, I., 1977. Frontier orbitals and organic chemical reactions. Wiley.

Fox Ramos, A.E., Alcover, C., Evanno, L., et al, 2017. Revisiting previously investigated plants: a molecular networking-based study of Geissospermum laeve. J. Nat. Prod. 80, 1007–1014.

Gao, L., Rutz, L., Schrenk, D., 2020. Structure-dependent hepatocytotoxic potencies of selected pyrrolizidine alkaloids in primary rat hepatocyte culture. Food Chem. Toxicol. 135, 110923.

Ghaffari, M., Bano, S., Hayat, K., 2013. Antimicrobial and phytotoxic effects of the plant Heliotropium dasycarpum L. Int. J. Pharm. Bio. Sci. 4, 339–345.

Ghaffari, M.A., Chaudhary, B.A., Uzair, M., et al, 2016. Cytotoxic, α-chymotrypsin and urease inhibition activities of the plant Heliotropium dasycarpum L. Afr. J. Tradit. Complement. Altern. Med. 13, 194–198.

Helfand, S.L., Werkmeister, J., Roder, J.C., 1982. Chemiluminescence response of human natural killer cells. I. The relationship between target cell binding, chemiluminescence, and cytolysis. J. Exp. Med. 156, 492–505.

Horchani, M., Hajlaoui, A., Harrath, A.H., et al, 2020. New pyrazolo-triazolo-pyrimidine derivatives as antibacterial agents: Design and synthesis, molecular docking and DFT studies. J. Mol. Struct. 1199, 127007.

Iwashina, T., Ootani, S., Hayashi, K., 1984. Neochilenin, a new glycoside of 3-O-methylquercetin, and other flavonols in the tepals

of Neochilenia, Neoporteria and Parodia species (Cactaceae). The botanical magazine= Shokubutsu-gaku-zasshi 97, 23–30.

Lazarova, I., Zengin, G., Bender, O., et al, 2015. A comparative study of Bulgarian and Turkish Asphodeline lutea root extracts: HPLC–UV profiles, enzyme inhibitory potentials and anti-proliferative activities against MCF-7 and MCF-10A cell lines. J. Funct. Foods 15, 254–263.

Mandić, B.M., Vlajić, M.D., Trifunović, S.S., et al, 2015. Optimisation of isolation procedure for pyrrolizidine alkaloids from Rindera umbellata Bunge. Nat. Prod. Res. 29, 887–890.

March, R.E., Miao, X.-S., 2004. A fragmentation study of kaempferol using electrospray quadrupole time-of-flight mass spectrometry at high mass resolution. Int. J. Mass Spectrometry 231, 157–167. https://doi.org/https://doi.org/10.1016/j.ijms.2003.10.008.

Miteva, M.A., Guyon, F., Tufféry, P., 2010. Frog2: Efficient 3D conformation ensemble generator for small compounds. Nucleic Acids Res. 38, W622–W627.

Moghimi, S., Goli-Garmroodi, F., Allahyari-Devin, M., et al, 2018. Synthesis, evaluation, and molecular docking studies of aryl urea-triazole-based derivatives as anti-urease agents. Arch. Pharm. 351, 1800005.

Morris, G.M., Huey, R., Lindstrom, W., et al, 2009. AutoDock4 and AutoDockTools4: Automated docking with selective receptor flexibility. J. Comput. Chem. 30, 2785–2791.

Myagchilov, A., Gorovoy, P., Sokolova, L., 2020. Flavonoids from Inflorescences of Synurus Deltoides. Chem. Nat. Compd. 56, 343–344.

Nibret, E., Sporer, F., Asres, K., et al, 2009. Antitrypanosomal and cytotoxic activities of pyrrolizidine alkaloid-producing plants of Ethiopia. J. Pharm. Pharmacol. 61, 801–808.

Ning, J., Chen, L., Strikwold, M., et al, 2019. Use of an in vitro–in silico testing strategy to predict inter-species and inter-ethnic human differences in liver toxicity of the pyrrolizidine alkaloids lasiocarpine and riddelliine. Arch. Toxicol. 93, 801–818.

Nothias, L.-F.l., Nothias-Esposito, M.l., da Silva, R., et al., 2018. Bioactivity-based molecular networking for the discovery of drug leads in natural product bioassay-guided fractionation. J. Nat. Prod. 81, 758–767.

Parveen, M., Azeem, M., Aslam, A., et al, 2022. Isolation, Identification, Spectral Studies and X-ray Crystal Structures of Two Compounds from Bixa orellana, DFT Calculations and DNA Binding Studies. Crystals 12, 380.

Ozdemir, U. O., Ilbiz, F., Gunduzalp, A. B., Ozbek, N., Genç, Z. K., Hamurcu, F., & Tekin, S. J. J. o. M. S. (2015). Alkyl sulfonic acide hydrazides: Synthesis, characterization, computational studies and anticancer, antibacterial, anticarbonic anhydrase II (hCA II) activities.1100, 464-474.

Parveen, S., Alnoman, R.B., Bayazeed, A.A., et al, 2020. Computational Insights into the Drug Repurposing and Synergism of FDA-approved Influenza Drugs Binding with SARS-CoV-2 Protease against COVID-19. Am. J. Microbiol. Res. 8, 93–102.

Pettersen, E.F., Goddard, T.D., Huang, C.C., et al, 2004. UCSF Chimera—a visualization system for exploratory research and analysis. J. Comput. Chem. 25, 1605–1612.

Rahman, J., Tareq, A.M., Hossain, M., et al, 2020. Biological evaluation, DFT calculations and molecular docking studies on the antidepressant and cytotoxicity activities of Cycas pectinata Buch.-Ham. Compounds. Pharmaceuticals. 13, 232.

Rahman, S.U., Adhikari, A., Ismail, M., et al., 2016. Beneficial Effects of Trillium govanianum Rhizomes in Pain and Inflammation. Molecules 21, https://doi.org/doi:10.3390/molecules21081095.

Reina, M., Mericili, A., Cabrera, R., et al, 1995. Pyrrolizidine alkaloids from Heliotropium bovei. Phytochemistry 38, 355–358.

Roeder, E., Bourauel, T., Neuberger, V., 1992. Symviridine, a new pyrrolizidine alkaloid from Symphytum species. Phytochemistry 31, 4041–4042.

Roeder, E., Wiedenfeld, H., Edgar, J., 2015. Pyrrolizidine alkaloids in medicinal plants from North America. Die Pharmazie-Int. J. Pharm. Sci. 70, 357–367.

Sarkar, C., Mondal, M., Khanom, B., et al, 2021. Heliotropium indicum L.: From Farm to a Source of Bioactive Compounds with Therapeutic Activity. Evidence-Based Complementary and Alternative Medicine. 2021,

Sayin, K., Üngördü, A., 2018. Investigation of anticancer properties of caffeinated complexes via computational chemistry methods. Spectrochim. Acta A Mol. Biomol. Spectrosc. 193, 147–155.

Schramm, S., Köhler, N., Rozhon, W., 2019. Pyrrolizidine alkaloids: biosynthesis, biological activities and occurrence in crop plants. Molecules 24, 498.

Seremet, O.C., Olaru, O.T., Gutu, C.M., et al, 2018. Toxicity of plant extracts containing pyrrolizidine alkaloids using alternative invertebrate models. Mol. Med. Rep. 17, 7757–7763.

Shafiei, A., Salimi, M., Farsam, H., et al, 2002. Pyrrolizidine alkaloids from Heliotropium dissitiflorum Boiss. Daru 10, 168–170.

Shimshoni, J.A., Barel, S., Mulder, P.P., 2021. Comparative risk assessment of three native Heliotropium species in Israel. Molecules 26, 689.

Shimshoni, J.A., Mulder, P.P., Bouznach, A., et al, 2015. Heliotropium europaeum poisoning in cattle and analysis of its pyrrolizidine alkaloid profile. J. Agric. Food Chem. 63, 1664–1672.

Singh, B., Sahu, P., Jain, S., et al, 2002. Antineoplastic and antiviral screening of pyrrolizidine alkaloids from Heliotropium subulatum. Pharm. Biol. 40, 581–586.

Singh, B., Sahu, P.M., Sharma, R.A., 2017. Flavonoids from Heliotropium subulatum exudate and their evaluation for antioxidant, antineoplastic and cytotoxic activities II. Cytotechnology 69, 103–115.

Sussman, J.L., Lin, D., Jiang, J., Manning, N.O., Prilusky, J., Ritter, O., Abola, E.E., 1998. Protein Data Bank (PDB): database of three-dimensional structural information of biological macromolecules. Acta Crystallographica Section D: Biological Crystallography 54 (6), 1078–1084.

Tahseen, G., Kalsoom, A., Faiz-ul-Hassan, N., et al, 2010. Screening of selected medicinal plants for urease inhibitory activity. Biol. Med. 2, 64–69.

Tao, A., Huang, Y., Shinohara, Y., et al, 2018. ezCADD: A rapid 2D/3D visualization-enabled web modeling environment for democratizing computer-aided drug design. J. Chem. Inf. Model. 59, 18–24.

Tareen, R.B., Bibi, T., Khan, M.A., et al, 2010. Indigenous knowledge of folk medicine by the women of Kalat and Khuzdar regions of Balochistan. Pakistan. Pak J Bot. 42, 1465–1485.

Valarmathi, T., Premkumar, R., Meera, M., et al, 2021. Spectroscopic, quantum chemical and molecular docking studies on 1-amino-5-chloroanthraquinone: A targeted drug therapy for thyroid cancer. Spectrochim. Acta A Mol. Biomol. Spectrosc. 255, 119659.

Wang, H., Xu, X., Wang, X., et al., 2022. An analytical strategy for discovering structural analogues of alkaloids in plant food using characteristic structural fragments extraction by high resolution orbitrap mass spectrometry. 154, 112329.

Woodley, S., 2018. A Literature Review of Chinese Herbal Medicine in the Treatment of Gastritis. https://stevewoodley.wordpress.com.

Zarren, G., Shafiq, N., Arshad, U., et al, 2021. Copper-catalyzed one-pot relay synthesis of anthraquinone based pyrimidine derivative as a probe for antioxidant and antidiabetic activity. J. Mol. Struct. 1227, 129668.

Zhao, Y., Xia, Q., Yin, J.J., et al, 2011. Photoirradiation of dehydropyrrolizidine alkaloids—formation of reactive oxygen species and induction of lipid peroxidation. Toxicol. Lett. 205, 302–309.